ACS central science

http://pubs.acs.org/journal/acscii

Research Article

Spontaneous Electric Fields Play a Key Role in Thermochemical Catalysis at Metal–Liquid Interfaces

Thejas S. Wesley, Yuriy Román-Leshkov,* and Yogesh Surendranath*

Cite This: https://doi.org/10.1021/acscentsci.1c00293

Read Online

ACCESS | Metrics & More | Article Recommendations | Supporting Information

ABSTRACT: Large oriented electric fields spontaneously arise at all solid–liquid interfaces via the exchange of ions and/or electrons with the solution. Although intrinsic electric fields are known to play an important role in molecular and biological catalysis, the role of spontaneous polarization in heterogeneous thermocatalysis remains unclear because the catalysts employed are typically disconnected from an external circuit, which makes it difficult to monitor or control the degree of electrical polarization of the surface. Here, we address this knowledge gap by developing general methods for wirelessly monitoring and controlling spontaneous electrical polarization at conductive catalysts dispersed in liquid media. By combining electrochemical and spectroscopic measurements, we demonstrate that proton and electron transfer from solution controllably, spontaneously, and wirelessly polarize Pt surfaces during thermochemical catalysis. We employ liquid-phase ethylene hydrogenation on a Pt/C catalyst as a thermochemical probe reaction and observe that the rate of this nonpolar hydrogenation reaction is significantly influenced by spontaneous electric fields generated by both interfacial proton transfer in water and interfacial electron transfer from organometallic redox buffers in a polar aprotic *ortho*-difluorobenzene solvent. Across these vastly disparate reaction media, we observe quantitatively similar scaling of ethylene hydrogenation rates with the Pt open-circuit electrochemical potential (E_{OCP}). These results isolate the role of interfacial electrostatic effects from medium-specific chemical interactions and establish that spontaneous interfacial electric fields play a critical role in liquid-phase heterogeneous catalysis. Consequently, E_{OCP}—a generally overlooked parameter in heterogeneous catalysis—warrants consideration in mechanistic studies of thermochemical reactions at solid–liquid interfaces, alongside chemical factors such as temperature, reactant activities, and catalyst structure. Indeed, this work establishes the experimental and conceptual foundation for harnessing electric fields to both elucidate surface chemistry and manipulate preparative thermochemical catalysis.

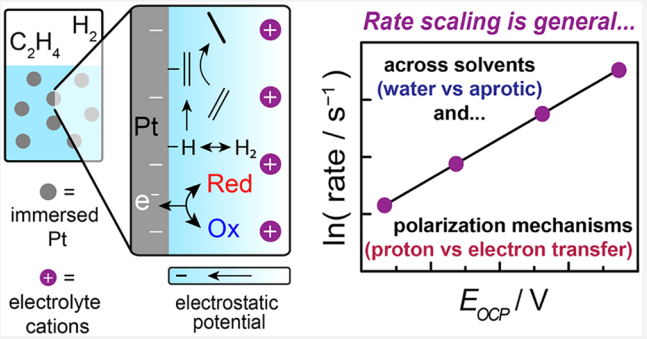

INTRODUCTION

Electric fields are known to play an important role in many catalytic transformations throughout chemistry[1−20] and biology.[21,22] For example, in molecular catalysis, charged moieties in the secondary sphere of a coordination compound can impart oriented internal electric fields,[11,13−15] which have been used to accelerate CO_2 activation (Figure 1, left).[11] Similarly, in enzymes, amino acid residues sustain enormous oriented electric fields within the active site that can drive biological catalysis (Figure 1, center).[21,22] In principle, oriented electric fields could also be used to control thermochemical catalysis at solid–liquid interfaces (Figure 1, right), which is playing an increasingly important role in facilitating the transition to a low-carbon energy and chemical economy.[23−30] Indeed, electrical charging or polarization arises spontaneously (i.e., without any external driving force) at *all* solid–liquid interfaces, creating large, intrinsically oriented electric fields at the interface.[31] Yet, this spontaneous electrical polarization is rarely considered or invoked in thermochemical catalysis, primarily for two reasons. First, it is difficult to

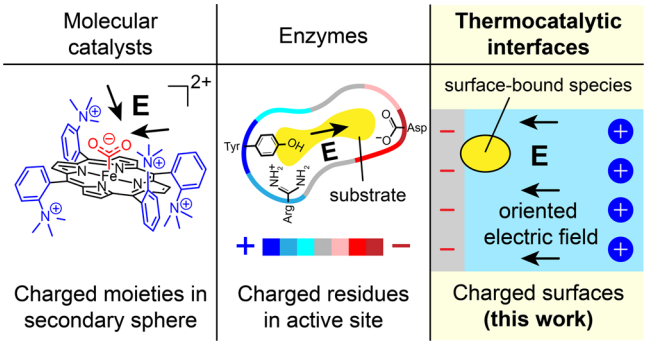

Figure 1. Spontaneous electric fields (**E**) in catalysis.

Received: March 3, 2021

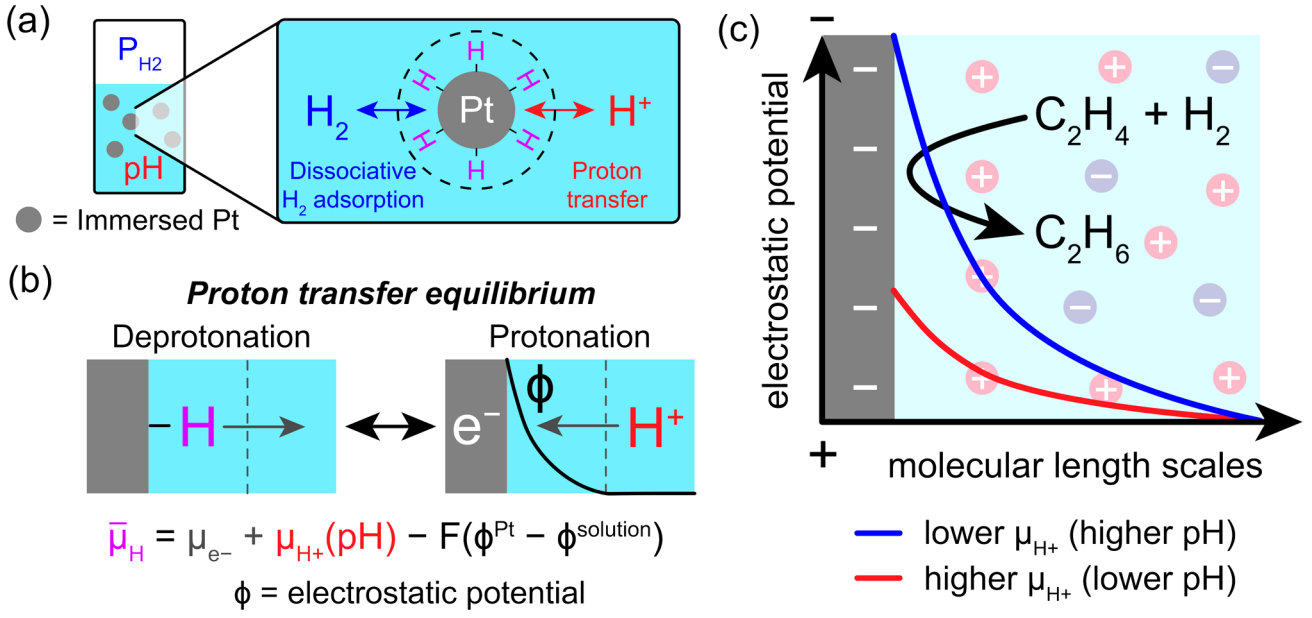

Figure 2. (a) Spontaneous interfacial reactions inherent to H_2-saturated Pt−water interfaces. (b) Electrochemical equilibrium for spontaneous interfacial proton transfer. $\bar{\mu}_H$ is the electrochemical potential of surface H*, and μ_{e-} and μ_{H+} are, respectively, the chemical potential of electrons in Pt and protons in solution. ϕ is the electrostatic potential (specifically, the Galvani potential). (c) Spontaneous proton transfer at Pt−water interfaces is expected to give rise to pH-dependent interfacial electric fields. We employ ethylene hydrogenation as a test reaction to probe the impact of spontaneous polarization on catalysis.

monitor electrical polarization at interfaces that are not connected to macroscopic wires. Such "distributed" interfaces, which include solid catalysts (e.g., supported metal nanoparticles) distributed throughout packed-bed or stirred-tank reactors, underpin virtually all of heterogeneous catalysis. Second, the heterogeneous catalysis community has historically focused on reactions at solid−gas interfaces, where electrical polarization is usually presumed to be negligible (though it is not necessarily so[4,32,33]). Yet, a general understanding of how spontaneous electrical polarization influences thermochemical reactivity could provide a powerful new handle—complementary to existing chemical principles—for understanding and controlling heterogeneous catalysis.

Electrical polarization of solid−liquid interfaces is most commonly studied within the context of electrochemistry. In this context, electrical polarization is controlled by passing charge through an external circuit driven by a power source (e.g., a potentiostat or battery). This driven polarization forms the basis for interconverting electrical and chemical energy in a wide array of electrochemical devices and is known at a molecular level to induce ion migration,[31] order solvents,[31,34−38] polarize adsorbates,[39−42] and alter the free energy and kinetics of adsorption.[31,43]

However, electrical polarization also arises *spontaneously* at all solid−liquid interfaces, even those entirely disconnected from any wires or electrical circuits. This phenomenon exists because differences in the chemical composition of the two phases can drive the spontaneous transfer of charged species (i.e., ions and/or electrons) across the interface. Specifically, the driving force for an interfacial charge transfer process is given by the difference in electrochemical potentials of the species involved.[31,44] By definition, the electrochemical potential, $\bar{\mu}_j^\alpha$, of species j in phase α, measures the total work required to differentially add 1 mole of species j to phase α. Therefore, $\bar{\mu}_j^\alpha$ depends on both chemical and electrostatic contributions and can be parsed as follows: $\bar{\mu}_j^\alpha = \mu_j^\alpha + zF\phi^\alpha$, where μ_j^α is the chemical potential of j in an uncharged reference phase, z is the charge number of species j, F is Faraday's constant, and ϕ^α is the electrostatic potential (specifically, the Galvani potential) of phase α.[31] Upon contacting the catalyst surface with solution, any difference between the chemical potentials of the charged species at the surface and in solution will drive spontaneous, incremental transfer of that charged species until an electrostatic potential difference, $\Delta\phi^{\text{surface−solution}} = \phi^{\text{surface}} - \phi^{\text{solution}}$, is generated that counteracts the chemical potential difference;[31] in this manner, electrochemical equilibrium is established. Such equilibration processes result in spontaneous electrical polarization of the solid−liquid interface, with attendant interfacial electric fields spanning molecular length-scales. Despite the long-standing appreciation that solid−liquid interfaces undergo spontaneous polarization,[31] this fundamental phenomenon has been largely ignored in understanding heterogeneous catalysis at solid−liquid interfaces.

Spontaneous polarization effects are expected to be especially pronounced for heterogeneous catalytic reactions occurring in aqueous media, because water is particularly effective at solvating ions and protons. For example, during Pt-catalyzed aqueous hydrogenation reactions, the adsorbed H* intermediates involved in product formation are also in equilibrium with protons in solution (Figure 2a). Indeed, under such conditions, H* undergoes reversible deprotonation to produce a solution-phase proton, leaving behind a residual electron equivalent in the Pt (and vice versa; Figure 2b). Accordingly, the electrochemical potential of H* on the surface must equal the combined electrochemical potentials of H^+ in bulk solution and electrons in the Pt:

$$\bar{\mu}_H^{\text{surface}} = \bar{\mu}_{H^+}^{\text{solution}} + \bar{\mu}_{e^-}^{\text{Pt}}$$

where $\bar{\mu}_{H^+}^{\text{solution}} = \mu_{H^+}^{\text{solution}} + F\phi^{\text{solution}}$ and $\bar{\mu}_{e^-}^{\text{Pt}} = \mu_{e^-}^{\text{Pt}} - F\phi^{\text{Pt}}$;[31] the electron chemical potential, $\mu_{e^-}^{\text{Pt}}$, depends on the chemical

https://doi.org/10.1021/acscentsci.1c00293
ACS Cent. Sci. XXXX, XXX, XXX−XXX

composition of the Pt, and thus relates to the Pt work function. We note that the foregoing equation is simply the Nernst condition of equilibrium and reflects both chemical and electrostatic factors.[31] In order to parse the two contributions, we may substitute in the expressions for $\bar{\mu}_{H^+}^{solution}$ and $\bar{\mu}_{e^-}^{Pt}$ in order to arrive at the following expression for the equilibrium condition:

$$\bar{\mu}_{H}^{surface} = \mu_{e^-}^{Pt} + \mu_{H^+}^{solution} - F\Delta\phi^{Pt-solution}$$

Consequently, in the limit that $\bar{\mu}_{H}^{surface}$ is constant—for example, when H* is quasi-equilibrated with H_2 gas held at constant pressure—and the chemical potential of electrons is invariant, increasing the solution pH (i.e., lowering $\mu_{H^+}^{solution}$) is expected to make $\Delta\phi^{Pt-solution}$ more negative in order to maintain equilibrium. In other words, a more alkaline medium will drive deprotonation of H* species (which are replenished and held at constant activity via H_2 dissociative chemisorption), leaving behind electrons in the metal that negatively charge the surface and sustain a pH-dependent interfacial electric field (Figure 2c). At H_2-saturated Pt−water interfaces, pH-dependent electrostatic potential drops have been quantified using non-faradaic interfacial probe reactions.[45] These electric fields have also been invoked to explain pH-dependent rates in electrocatalysis.[36]

Despite the foregoing understanding, the role of polarization in thermochemical heterogeneous catalysis at metal−water interfaces remains ambiguous. While studies have invoked that spontaneous electric fields may influence catalysis,[46−49] chemical effects convolute putative electrostatic contributions in these systems. For example, during the hydrogenation of maleic acid at a wired Pt−water interface, changes in rate with H_2 pressure were attributed to spontaneous electrical polarization, without accounting for changes in chemical driving force (i.e., the H_2 reaction order).[46] Likewise, pH-dependent CO oxidation[47,48] and phenol hydrogenation[49] rates were indirectly attributed to spontaneous polarization on the basis of shifts in the CO infrared spectrum and molecular dynamics simulations, respectively, but could not rule out contributions from chemical pH effects. Thus, it remains unclear whether spontaneous electrical polarization indeed plays a role in liquid-phase thermochemical heterogeneous catalysis.

To address this knowledge gap, we herein develop general methods for monitoring and controlling spontaneous electrical polarization during catalysis at distributed metal−liquid interfaces. By combining electrochemical and spectroscopic measurements, we demonstrate that different classes of reversible redox partners deployed in solution controllably, spontaneously, and wirelessly polarize distributed Pt surfaces during thermochemical catalysis. We employ ethylene hydrogenation as a probe reaction (Figure 2c) in order to minimize the influence of acid−base reactions and find that the rate of this nonpolar hydrogenation reaction is significantly influenced by spontaneous electric fields generated by both interfacial proton transfer in water and interfacial electron transfer in a polar aprotic *ortho*-difluorobenzene solvent. These results isolate the role of interfacial electrostatic effects from medium-specific chemical interactions and establish that spontaneous interfacial electric fields play a critical role in liquid-phase heterogeneous catalysis.

RESULTS AND DISCUSSION

Infrared Stark Spectroscopy to Probe Spontaneous Polarization at Distributed Pt−Water Interfaces. Investigating the influence of spontaneous electrical polarization on thermochemical catalysis requires, first, a method for tracking the magnitude of interfacial polarization at distributed metal−liquid interfaces across reaction conditions. Unfortunately, it is not possible to directly quantitate electric fields or $\Delta\phi$ at metal−liquid interfaces by electrochemical methods. This is because electrochemical methods measure electrochemical potentials (i.e., $\bar{\mu}$), which inherently *combine* chemical and electrostatic factors.[31,50] Therefore, although macroscopic electrodes allow for convenient electrochemical sensing, it cannot be assumed *a priori* that changes in the electrochemical potential, *E*, relative to a constant reference couple, translate into changes in $\Delta\phi$ across a metal−liquid interface. Furthermore, the inability to make an electrical contact to a distributed interface necessitates a nonelectrochemical probe of the interfacial electric field.

In order to track changes in the degree of spontaneous polarization at a distributed Pt−liquid interface (i.e., Pt/C immersed in buffered aqueous electrolytes), we employ adsorbed CO as an interface-specific vibrational reporter in attenuated total reflectance (ATR)-infrared (IR) spectroscopy. The CO stretching frequency, ν(CO), is sensitive to interfacial polarization;[40,51−54] this phenomenon, termed a Stark shift, has been ascribed to surface charge affecting back-bonding into CO π^* orbitals.[40,55] Since CO adsorbs strongly to Pt surfaces, these Stark shifts sample changes in the degree of polarization at a distributed Pt−liquid interface as a function of changes in the electrolyte composition. In order to correlate these Stark shifts to the electrochemical potential of the medium, we separately monitored the open-circuit potentials (E_{OCP}) of a macroscopic Pt sensing electrode under identical conditions. To ensure stable polarization via H_2/H^+ equilibration, the system was simultaneously saturated with H_2 (in addition to CO) across all conditions.

At pH 5, we observe an IR absorption peak at 2046 cm^{-1}, which corresponds to atop-bound CO, $\nu(CO_A)$ (Figure 3a, red).[40,47,51,52,54,56−58] The pronounced bipolar shape of the atop CO feature has been commonly observed for infrared reflectance measurements of CO adsorbed on carbon-supported metal nanoparticles and has been ascribed to optical effects.[57,59−62] As the pH is increased to 7 (Figure 3a, black) and 9 (Figure 3a, blue), $\nu(CO_A)$ redshifts to 2041 and 2035 cm^{-1}, respectively. Importantly, since the bipolar peak shape is preserved across the pH range investigated, this optical artifact would minimally convolute the extracted trends in peak position. We note that, depending on pH, we also observe a broad bridge-bound CO feature (Figure S2), consistent with prior studies;[40,47,54,56,57,62] however, due to its breadth and convolution from water vapor, we refrain from analyzing this feature. However, the data clearly indicate a systematic redshift in $\nu(CO_A)$ as the solution pH is increased.

In order to determine whether E_{OCP} of a macroscopic sensing electrode provides a faithful proxy for the degree of polarization at the distributed Pt/C particles, we dropcast the same Pt/C catalyst onto carbon paper (referred to hereafter as Pt/C electrodes). Under conditions identical to the ATR measurements, we observe a linear pH-dependence of E_{OCP} of the Pt/C electrodes in the presence of CO and H_2 (Figure S3, black squares); however, this scaling deviates from what is

https://doi.org/10.1021/acscentsci.1c00293
ACS Cent. Sci. XXXX, XXX, XXX−XXX

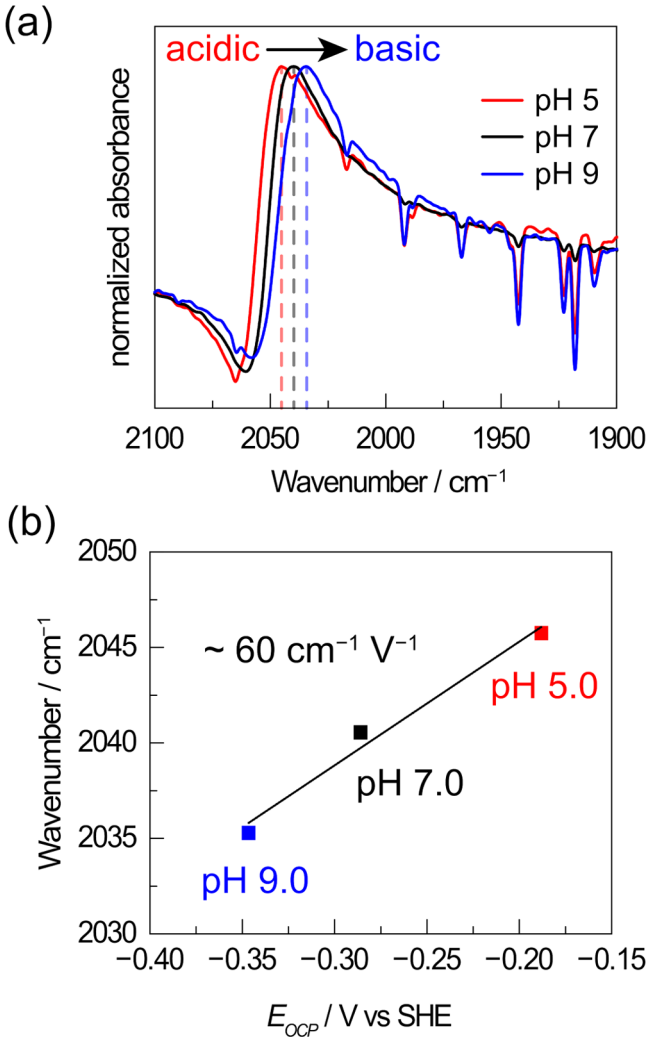

Figure 3. (a) pH-dependence of ATR-IR spectra, taken at saturation, of atop-bound CO at a distributed Pt−water interface (i.e., Pt/C immersed in buffered aqueous electrolytes). (b) Peak maximum for atop-bound CO vs open-circuit potentials (E_{OCP}) of a Pt/C electrode. Conditions: 7 kPa CO, 94 kPa H_2, 60 wt % Pt/C, electrolyte = 0.5 M $NaClO_4$ in Britton−Robinson universal buffer (0.04 M acetic acid, 0.04 M phosphoric acid, 0.04 M boric acid in water); pH adjusted with NaOH. Performed at room temperature (294 ± 1 K).

expected from the Nernst equation (Figure S3, gray circles). Because E_{OCP} is the potential that exactly balances anodic and cathodic processes, the non-Nernstian behavior observed in the presence of CO may be readily explained by the differential impact of site-blocking CO on the kinetics of H_2 oxidation and H^+ reduction half-reactions. Nonetheless, a plot of $\nu(CO_A)$ vs E_{OCP} is linear (Figure 3b) and provides an *inferred* electrochemical Stark tuning slope of approximately ~60 cm^{-1} V^{-1} for the adsorbed CO species across the distributed Pt−water interface. Although we refrain from quantitative interpretation of this slope because of the inherent complexities of the system (see supplementary information, SI, section 2.1 for a detailed discussion), this value is in line with the relatively wide (i.e., 25−62 cm^{-1} V^{-1}) range of Stark tuning values reported for CO on Pt under driven (i.e., wired) polarization.[40,51−54,62]

We note that other possible chemical contributions to changes in $\nu(CO_A)$ are inconsistent with the observed trend. In particular, the decreasing proton activity with increasing pH would be expected to attenuate H-bonding interactions (e.g., a CO−H^+ adduct), but as previously discussed this effect would be expected to blueshift the CO stretching frequency.[47] This is at odds with the observed red shift. Additionally, although OH^- coadsorption might influence the CO band, the observed changes in E_{OCP} nearly offset changes in OH^- activity and OH^- adsorption is disfavored at the reducing potentials recorded here in the presence of CO and H_2.[63] Finally, although both $\nu(CO_A)$ and Stark tuning slopes are known to depend on CO coverage,[52] electrochemical CO stripping experiments performed on the Pt/C catalyst under conditions mimicking the ATR measurements (see SI section 1.2.3 for full details) demonstrate that the CO coverage is roughly constant at a value of ~1 across the pH range spanned by our IR experiments (Figures S4−S5 and Table S2; see SI section 2.2 for a detailed discussion). This suggests that the observed shift in $\nu(CO_A)$ with pH likely does not arise from pH- or buffer speciation-induced changes to the equilibrium CO coverage.

Based on the foregoing analysis, we ascribe the pH-dependence of $\nu(CO_A)$ to a progressive increase in the magnitude of spontaneous electrical polarization of the distributed Pt−water interface with increasing solution alkalinity. Additionally, these studies imply that, for this system, E_{OCP} as measured by a macroscopic sensing electrode provides a good estimate of changes in the magnitude of spontaneous polarization (i.e., changes to $\Delta\phi$) across a distributed Pt−water interface, consistent with prior work.[45]

Tracking Spontaneous Polarization during Ethylene Hydrogenation at Distributed Pt−Water Interfaces. The above observations indicate that the degree of spontaneous polarization of a Pt−water interface can be tuned simply by varying the pH. Thus, we envisioned that the pH-dependence of a model heterogeneous thermochemical reaction could provide insight into the role of interfacial electric fields in catalysis. For these studies, we elected to examine the pH/potential-dependence of Pt/C catalyzed ethylene hydrogenation in aqueous media. This explicitly nonpolar transformation is expected to provide a baseline measure of electrostatic contributions to catalysis that would only be amplified for reactions of more polar substrates.

Experiments were carried out using a well-mixed slurry reactor equipped with a Pt sensing wire and reference electrode, which provided an *operando* measurement of Pt E_{OCP} during catalysis (Figure 4); we note that similar approaches have been used before.[64,65] A Pt wire was chosen for this purpose in order to minimize background catalytic activity. Moreover, because ethylene hydrogenation is structure-insensitive across the entire range spanning fully dispersed Pt/SiO_2 (i.e., all Pt atoms accessible to titration by H_2) to a Pt wire,[66] any impact of olefin surface chemistry on electrochemical pinning reactions would be expected to be similar on both Pt/C and the Pt sensing wire. During the reaction, ethylene (5 kPa) and hydrogen (96 kPa) gases were continuously sparged through the aqueous electrolyte containing suspended Pt/C catalyst particles (Figure 4). The pH was adjusted with $HClO_4$, NaOH, or a dilute borate buffer, and $NaClO_4$ was added as a supporting electrolyte to maintain 0.1 M total ionic strength. Importantly, under these conditions, the Pt sensing wire contributed negligibly to measured hydrogenation rates (Figure S6). Thus, measured rates reflect the catalytic activity of the dispersed Pt/C particles.

Care was taken to ensure that measured rates reflect intrinsic reaction kinetics. Specifically, ethylene hydrogenation rates

https://doi.org/10.1021/acscentsci.1c00293
ACS Cent. Sci. XXXX, XXX, XXX−XXX

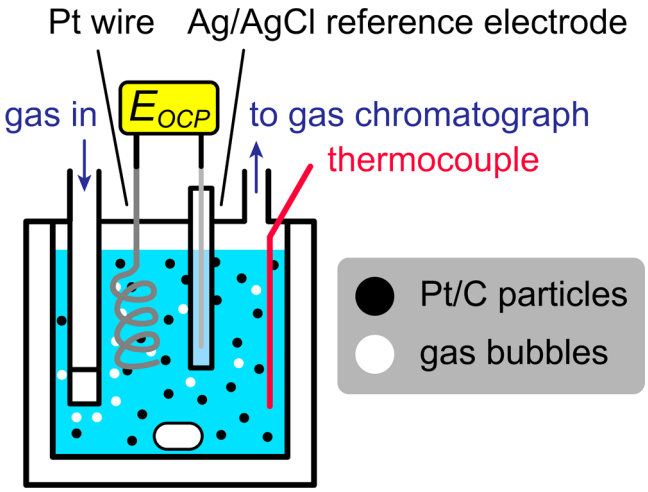

Figure 4. Diagram of the well-mixed slurry reactor used to monitor spontaneous electrical polarization during liquid-phase ethylene hydrogenation catalysis. E_{OCP} refers to the open-circuit potential of the Pt wire vs the Ag/AgCl reference electrode.

were measured at differential ethylene conversion and corrected for first-order deactivation (Figure S7). We report turnover rates, defined herein as the rate of ethane production per surface Pt atom as estimated from Pt loading and particle size distributions (see SI section 1.3 and Figure S8). Importantly, absolute hydrogenation rates scaled proportionally to catalyst loading (Figure S9), indicating negligible gas-to-liquid interphase mass transfer limitations.[67] Moreover, turnover rates were unaffected by Pt loading on the carbon support (Table S3), demonstrating that internal diffusion limitations are negligible within the catalyst pores.[68,69] Taken together, the latter two observations establish that our rate measurements are free from mass transfer artifacts and thus reflect intrinsic liquid-phase ethylene hydrogenation kinetics.

Aqueous ethylene hydrogenation rates decrease systematically with increasing pH. At pH = 2.0, we observe a hydrogenation rate of 3.0 ± 0.2 s^{-1} (Figure 5a), which is similar to the gas-phase rate (i.e., 3.0 s^{-1}) at 273 K and similar C_2H_4 and H_2 partial pressures, as inferred from previously measured rates and reaction orders.[66] However, upon increasing the pH to 5.1, 9.0, and 12.9, the rate systematically decreases to 2.4 ± 0.1, 1.6 ± 0.3, and 1.0 ± 0.01 s^{-1} respectively (Figure 5a). These changes constitute an

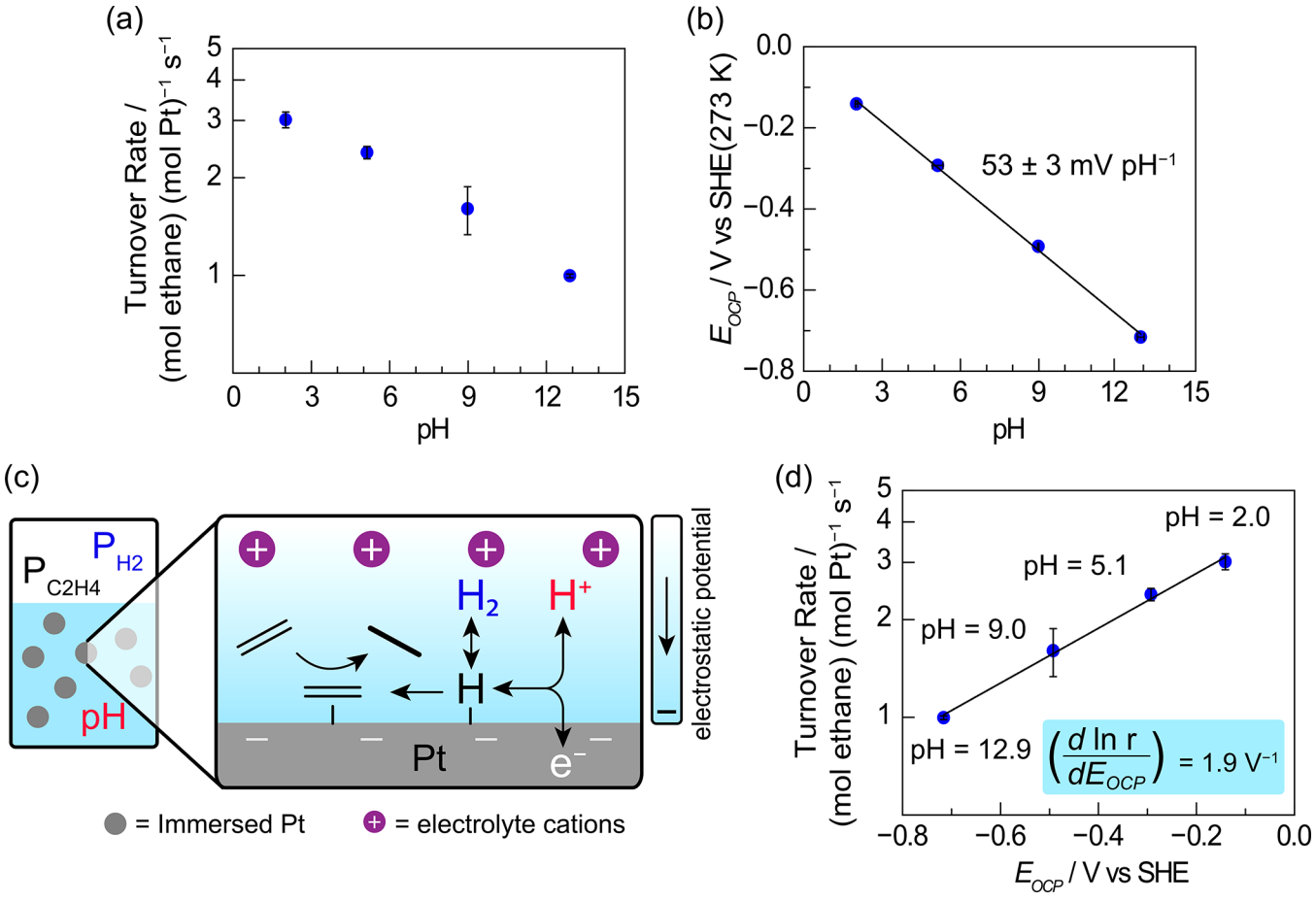

Figure 5. Ethylene hydrogenation in aqueous electrolytes on a Pt/C catalyst. (a) pH-dependence of aqueous ethylene hydrogenation turnover rates (note logarithmic *y*-axis). (b) pH-dependence of the steady-state open-circuit potential (E_{OCP}) of a Pt wire during aqueous ethylene hydrogenation. (c) Pt−water interfaces are spontaneously polarized by proton transfer during and in parallel to ethylene hydrogenation catalysis. (d) E_{OCP}-dependence of aqueous ethylene hydrogenation turnover rates (note logarithmic *y*-axis). Conditions: 273 K, 5 kPa C_2H_4, 96 kPa H_2, 0.24 wt % Pt/C, solvent = 0.09−0.1 M $NaClO_4$ in water, 0.1 M total ionic strength. pH adjusted as follows: pH 2.0 ± 0.1 = 0.01 M $HClO_4$, pH 5.1 ± 0.2 = nothing added, pH 9.0 ± 0.02 = 10 mM borate buffer, pH 12.9 ± 0.1 = 0.01 M NaOH. Uncertainties in rates and pH values reflect standard deviations of independent trials. Note: At 273 K, $pK_w = 10^{-15}$, so pH ranges from 0−15 and neutral water is pH = 7.5.

https://doi.org/10.1021/acscentsci.1c00293
ACS Cent. Sci. XXXX, XXX, XXX−XXX

exponential decrease in rate with increasing pH (Figure 5a). This trend of decreasing hydrogenation rates with increasing pH has also been observed for phenol hydrogenation.[49] In contrast to the hydrogenation of polar, protic phenol, which could be subject to Brønsted acid−base chemistry or promotion, the explicitly nonpolar nature of ethylene hydrogenation argues against a simple acid−base rationalization for the pH-dependence observed here. Moreover, the log−linearity of rate vs pH across 11 orders of magnitude in proton activity argues against a simple site-blocking model involving hydroxide ions. Finally, we note that the consistency in trend between unbuffered (pH 2.0, 5.1, 12.9) and borate-buffered (pH 9.0) electrolytes suggests that the borate buffer species do not significantly influence catalysis; this is consistent with the innocence of borate buffers in proton-coupled electron transfer at a Au−water interface.[70] Together, the data establish that aqueous, Pt/C-catalyzed ethylene hydrogenation rates exponentially decrease with increasing pH, in a manner inconsistent with simple acid−base or hydroxide site-blocking explanations.

The Pt wire sensing electrode provides a real-time estimate of changes in the polarization of the distributed Pt/C catalysts during the reaction and across conditions (see above). For unbuffered electrolytes (pH 2.0, 5.1, 12.9), Pt E_{OCP} values drift less than 8 mV during the initial stages of reaction (∼25 min) before reaching a steady-state value that varied by less than ∼2 mV over the remainder of the experiment (Figure S10a, b, d). For the borate-buffered electrolyte (pH 9.0), Pt E_{OCP} cathodically drifts ∼30 mV during the initial 80 min of reaction (which may, in part, stem from gradual changes to boron speciation and/or trace boric acid evaporation[71]), before stabilizing within a range of ∼2 mV (Figure S10c). The steady-state E_{OCP} values for all four conditions were found to be linearly dependent on pH with a slope of −53 ± 3 mV per pH unit versus the pH-independent (i.e., constant) standard hydrogen reference electrode (Figure 5b). Notably, this value is within error of the expected scaling of −54 mV per pH unit from the Nernst equation for H_2/H^+ interconversion at 273 K. This observation implies that, while ethylene hydrogenation is taking place, the Pt surface is simultaneously catalyzing the rapid interconversion of H^+ and H_2 (Figure 5c). This is consistent with prior work on the Pt-catalyzed hydrogenation of an unsaturated diol[45] and implies that the olefin hydrogenation minimally perturbs hydrogen evolution/oxidation catalysis. This in turn could reflect the fact that liquid water has been observed to mitigate formation of site-blocking ethylidyne during ethylene hydrogenation on Pt.[72] These E_{OCP} data establish that, during aqueous ethylene hydrogenation catalysis, varying the solution pH directly alters the degree of spontaneous polarization at the Pt−water interface.

Importantly, this electrochemical link between pH and E_{OCP} implies that the magnitude of spontaneous interfacial polarization is *inextricably* tied to an increase in solution alkalinity. Thus, it is possible that the observed pH-dependence of ethylene hydrogenation is actually a manifestation of a polarization-dependence of the reaction, which is induced by pH changes. Indeed, the ethylene hydrogenation rates scale exponentially with Pt E_{OCP} (Figure 5d; see below for detailed discussion of the slope), suggesting that E_{OCP} and pH are equally viable descriptors of ethylene hydrogenation rates in water.

Spontaneous Polarization of a Distributed Pt−Liquid Interface via Electron Transfer. Given that changes in pH and E_{OCP} are inextricably linked in aqueous electrolytes, we sought to deconvolute pH and electrostatic effects by employing an orthogonal class of charge transfer reactions—outer-sphere electron transfer (OSET)—to spontaneously polarize a Pt−liquid interface in an aprotic electrolyte.

In these experiments, we deployed metallocene-based redox buffers to drive polarization via OSET in an *ortho*-difluorobenzene (*o*-DFB) solvent. *o*-DFB was chosen not only because it is relatively noncoordinating and effective at solvating electrolytes,[73] but also because it is relatively inert with respect to hydrogenation. The redox buffers employed were decamethylferrocene (DMFc), decamethylmanganocene (DMMc), cobaltocene (Cc), and decamethylcobaltocene (DMCc), along with their respective one-electron oxidized hexafluorophosphate salts (Figure 6a). Whereas changes in proton activity served to tune the degree of polarization in water, here the degree of polarization is tuned by virtue of the distinct standard reduction potentials of the metallocene couples employed. Indeed, the family of metallocenes employed here display standard reduction potentials that span 1.4 V at 273 K (Figure S11, Table S4), providing a considerably larger range than the 0.81 V (i.e., [0.054 V per pH unit] × [15 pH units]) spontaneous polarization window accessible via pH variation in water at 273 K.

Rate measurements in *o*-DFB were performed largely analogously to our aqueous rate measurements. Specifically, solutions contained 0.2 M tetrabutylammonium hexafluorophosphate ($TBAPF_6$) as the supporting electrolyte, 1 mM of the metallocenium hexafluorophosphate salt, and either 2 mM (for Cc, DMMc, and DMFc) or 6 mM (for DMCc) metallocene. Activities of dissolved ethylene and H_2 were kept the same as in the aqueous measurements by using the same partial pressures of each gas (i.e., 5 and 96 kPa, respectively). These nonaqueous measurements are highly sensitive to trace quantities of water and O_2 and were performed with careful solvent drying and rigorously air-free techniques (see SI section 1.6 for full experimental details.) The electrochemical cell depicted in Figure 4 was augmented with a glassy carbon (GC) electrode (Figure S12). Because glassy carbon does not activate H_2, it only engages in outer-sphere electron exchange with the metallocene redox buffer. Consequently, the glassy carbon open-circuit potential (GC E_{OCP}) reports on the metallocene redox buffer ratio in solution, as given by the Nernst equation, without convolution from any hydrogen-mediated polarization contributions. Thus, GC E_{OCP} here serves a role analogous to that of pH in the aqueous measurements.

Metallocene redox buffers in solution effectively "pin" the electrochemical potential of electrons in Pt during ethylene hydrogenation catalysis. Specifically, with DMFc, DMMc, and Cc redox buffers, Pt and GC E_{OCP} values are equal throughout the reaction duration, and drift less than 4 mV with time-on-stream (Figures S13 − S15). With DMCc, Pt and GC E_{OCP} values are also nearly identical with time-on-stream, but drift anodically by ∼60 mV during the first hour on-stream before stabilizing (Figure S16). This transient in GC E_{OCP}, specifically, implies an increase in the ratio of $DMCc^+$ to DMCc; however, this leads to only a modest deviation in E_{OCP} from the Nernstian potential expected from the initial metallocene concentrations (Figure S17). Regardless, for all four metallocene redox buffers, steady-state Pt E_{OCP} values are pinned to within ∼3 mV of GC E_{OCP} values (Figure 6b). These results establish that Pt is essentially perfectly polarized during

https://doi.org/10.1021/acscentsci.1c00293
ACS Cent. Sci. XXXX, XXX, XXX−XXX

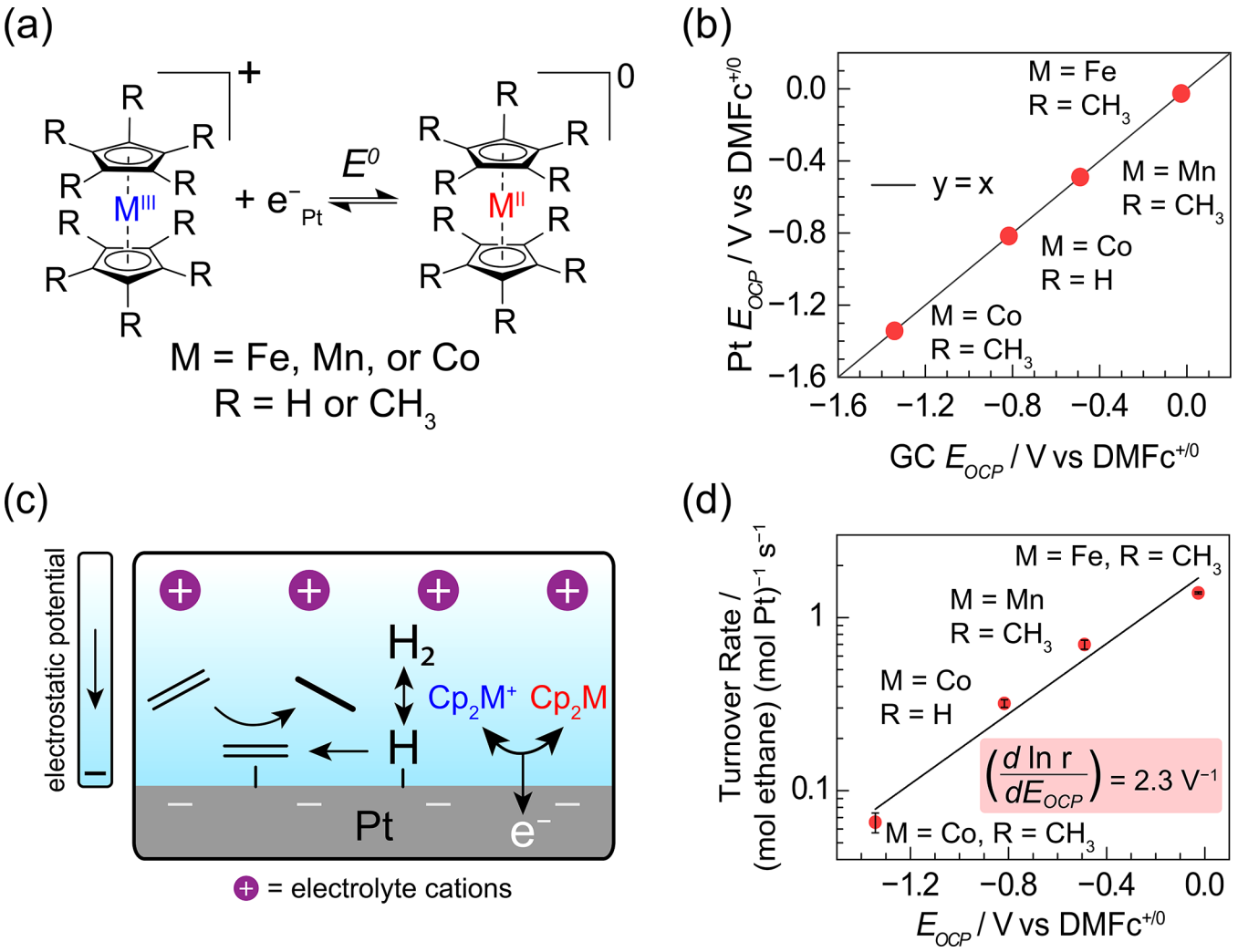

Figure 6. Ethylene hydrogenation in *ortho*-difluorobenzene (*o*-DFB) electrolytes on a Pt/C catalyst. (a) Metallocene-based outer-sphere electron transfer reactions used to spontaneously polarize Pt during ethylene hydrogenation catalysis in *o*-DFB. (b) Steady-state Pt open-circuit potentials (Pt E_{OCP}) vs glassy carbon open-circuit potentials (GC E_{OCP}) during ethylene hydrogenation catalysis. (c) Pt−(*o*-DFB) interfaces are spontaneously polarized via outer-sphere electron transfer during and in parallel to ethylene hydrogenation catalysis. (d) Pt E_{OCP}-dependence of ethylene hydrogenation turnover rates in *o*-DFB electrolytes (note logarithmic *y*-axis). Conditions: 273 K, 5 kPa C_2H_4, 96 kPa H_2, 0.21 wt % Pt/C, electrolyte = 0.2 M tetrabutylammonium hexafluorophosphate in *o*-DFB. Metallocene concentration = 2 or 6 mM; metallocenium hexafluorophosphate concentration = 1 mM. DMFc = decamethylferrocene (M = Fe, R = CH_3). Error bars reflect standard deviations from independent trials.

ethylene hydrogenation catalysis to be in electronic equilibrium with the solution-phase activities of reduced and oxidized metallocene equivalents (Figure 6c).

Furthermore, ATR-IR experiments indicate that metallocene-driven changes to Pt E_{OCP} correspond to changes in the degree of spontaneous polarization at the Pt−(*o*-DFB) interface. Specifically, the peak maximum of $\nu(CO_A)$ redshifts from 2056 cm^{-1} with a DMFc redox buffer to 2026 cm^{-1} with a more reducing DMMc redox buffer (Figure S18, Table S5). This two-point comparison corresponds to a Stark shift of approximately ∼60 cm^{-1} V^{-1}. The consistency between our aqueous and nonaqueous Stark shifts agrees with the similarity across solvents reported for CO Stark tuning on a polycrystalline Pt disk with driven polarization.[74] Although Stark tuning experiments have not, to our knowledge, been reported in *o*-DFB, our Stark shift exceeds by ∼3-fold values reported in the same study for similar polar aprotic electrolytes containing tetraalkylammonium salts.[74] Akin to our aqueous results, this difference may be attributable to Pt particle size or CO coverage effects, or convolution from the large negative-going feature of the bipolar peak (see SI section 2.1 for further discussion). While these potential sources of convolution preclude a quantitative analysis of the Stark tuning slopes, the data strongly indicate that the metallocene OSET method employed here effectively spontaneously polarizes the distributed Pt/C interface. In this regard, we stress that the similarity in Pt and GC E_{OCP} values during catalysis does not imply that $\Delta\phi$ is similar at the Pt−(*o*-DFB) and GC−(*o*-DFB) interfaces; indeed, $\Delta\phi$ at the respective interfaces would deviate in accordance with the difference between the electron chemical potentials (i.e., work functions) for Pt and GC.

During catalysis in *o*-DFB, ethylene hydrogenation rates systematically decrease with metallocene-driven, negative spontaneous polarization. In the presence of a DMFc redox buffer (steady-state Pt E_{OCP} = −0.03 V vs $DMFc^{+/0}$), a rate of 1.4 ± 0.02 s^{-1} was observed (Figure 6d). However, upon negative spontaneous polarization via DMMc (Pt E_{OCP} = −0.49 V vs $DMFc^{+/0}$), Cc (Pt E_{OCP} = −0.82 V vs $DMFc^{+/0}$),

https://doi.org/10.1021/acscentsci.1c00293
ACS Cent. Sci. XXXX, XXX, XXX−XXX

and DMCc (Pt E_{OCP} = −1.34 V vs $DMFc^{+/0}$) redox buffers, rates systematically decrease to 0.70 ± 0.04, 0.32 ± 0.02, and 0.066 ± 0.01 s^{-1} (Figure 6d). This trend constitutes an exponential decrease in rate with decreasing Pt E_{OCP}, consistent with our aqueous rate measurements.

We note that the observed trend in rate cannot be ascribed to site-blocking due to metallocene adsorption on the Pt surface. Indeed, the metallocene buffer concentration does not appear to influence observed rates, as we observe an ethylene hydrogenation rate of 0.66 s^{-1} in the presence of a 2.5-fold higher DMMc buffer concentration. This invariance in rate with DMMc buffer concentration (i.e., 0.70 ± 0.04 vs 0.66 s^{-1}), coupled with (1) the fact that the metallocenes share similar chemical structures and (2) the observation that the rate in the presence of the DMFc redox buffer is within ∼50% of the previously reported gas-phase rate,[66] suggests that metallocenes do not significantly block catalytic Pt sites in this system. We note, however, that this is not necessarily true for all classes of redox buffers; whether or not a redox buffer might interfere with catalysis would in general depend not only on redox buffer class but also on factors such as the solvent, catalyst, and catalytic reaction mechanism.

In view of the negligible site-blocking of metallocene redox buffers, the observation that ethylene hydrogenation is strongly and similarly sensitive to polarization across two distinct solvents (water vs *o*-DFB) and polarization mechanisms (proton transfer vs electron transfer) leads us to conclude that, even in water, E_{OCP}, rather than pH, is the controlling variable.

Comparison of Spontaneous Polarization-Dependence of Ethylene Hydrogenation in Aqueous and Nonaqueous Media. The foregoing data establish that, even though ethylene hydrogenation is a redox neutral, thermochemical reaction, it is nonetheless highly sensitive to the electrochemical potential of the interface. The data further indicate that "pinning" the electrochemical potential of the Pt surface via either proton transfer in water or outer-sphere electron transfer in *o*-DFB leads to a log−linear scaling between rate and catalyst potential (Figures 5d and 6d) across a wide range of 0.58 V in water and 1.31 V in *o*-DFB. These data strongly support the notion that the electrochemical potential (i.e., E_{OCP}) of the catalyst, a generally overlooked parameter in thermochemical catalysis, dramatically influences reaction rates at solid−liquid interfaces.

The slopes of these semilog rate vs E_{OCP} plots provide quantitative insight into the magnitude of interfacial polarization effects on thermochemical catalysis. In particular, these semilog plots provide what we define as an *apparent electrochemical activation slope*, S_{AEA},

$$S_{AEA} \triangleq \left(\frac{\partial \ln r}{\partial E_{OCP}}\right)_{T,P_{C2H4},P_{H2}}$$

which provides a quantitative measure of the susceptibility of a reaction rate to changes in the electrochemical potential (i.e., E_{OCP}) of the catalyst. A similar quantity has been previously defined for the electrochemical promotion of catalysis at solid−gas interfaces.[75,76] Notably, we observe that S_{AEA} = 1.9 V^{-1} for Pt-catalyzed ethylene hydrogenation in aqueous media (Figure 5d), which is similar to the value of 2.3 V^{-1} observed in *o*-DFB electrolytes with metallocene-based spontaneous polarization (Figure 6d). Although ethylene hydrogenation is a redox neutral reaction, these S_{AEA} values may nonetheless be converted into an equivalent Tafel slope, which is commonly used to analyze the potential-dependence of a charge transfer reaction:

$$\text{Tafel slope} \triangleq \left(\frac{\partial E}{\partial \log_{10} r}\right) = \frac{\ln 10}{S_{AEA}}$$

This analysis returns equivalent Tafel slopes of 1200 and 1000 mV $decade^{-1}$ for water and *o*-DFB electrolytes, respectively. These values are an order-of-magnitude larger than those typically observed for faradaic charge transfer reactions, which typically span from 30 to 200 mV depending on the mechanism of catalyzed charge transfer.[77] The substantially larger effective Tafel slopes observed here for thermocatalytic ethylene hydrogenation indicate that far greater electrical polarization is required to effect the same change in ethylene thermochemical hydrogenation rate as for a faradaic reaction. This in turn implies that the kinetically relevant elementary steps of liquid-phase ethylene hydrogenation depend far more on the properties of neutral molecules than on charged species (i.e., electrons and/or ions). While ethylene hydrogenation is far less potential-dependent than an electrochemical (i.e., charge transfer) reaction, we stress that in contrast to an electrochemical reaction, changes in *E* do *not* alter the overall reaction free energy of thermochemical ethylene hydrogenation. Indeed, since no current is flowing, the changes in reaction rate observed here arise without any additional energy flux to the system.

Although a detailed mechanistic analysis of the origin of these polarization effects is beyond the scope of this initial report, the quantitative similarity in S_{AEA} across vastly different reaction media and spontaneous polarization mechanisms implies that electrostatic effects are largely independent of the specific chemical constituents in the reaction medium. We note that a "local short-circuit" model,[65,78−81] wherein balancing H_2 oxidation and ethylene reduction half-reactions take place at the same interface, cannot explain these results because of the lack of proton donors in the nonaqueous measurements. Instead, although changes in E_{OCP} do not alter the overall thermodynamic reaction driving force for ethylene hydrogenation, the interfacial electric field can alter the affinity of the surface for polar solvent molecules[31,36] and augment the population and energies of surface intermediates and transition states, particularly those with dipolar character;[4,31,33,39,49,82] these effects, in essence, reflect electrostatic nonidealities inherent to the thermodynamics of condensed-matter interfaces.

We note that this electrostatic phenomenology appears, at least for this system, to dwarf chemical solvation effects on catalytic rates. Indeed, ethylene hydrogenation rates measured under liquid-phase conditions at modest polarization (this study) are within ∼50% of previously reported gas-phase rates,[66] implying that chemical solvation of surface species does not play a significant role under these conditions.[83] However, in contrast to the minimal chemical solvation effect, electrostatic polarization appears to have a significant impact on rate—for example, up to a 21-fold change in *o*-DFB—with increasing polarization attenuating rates relative to the gas-phase value.

Given the strong polarization dependence we observe for what is, ostensibly, one of the most nonpolar surface reactions, these studies suggest that spontaneous electrical polarization

https://doi.org/10.1021/acscentsci.1c00293
ACS Cent. Sci. XXXX, XXX, XXX−XXX

may play a general role in defining the rates of a diverse array of thermochemical transformations at metal−liquid interfaces.

CONCLUSION

The studies described herein establish that spontaneous electrical polarization, a property inherent to all solid−liquid interfaces, plays an important role in governing reaction rates in thermochemical heterogeneous catalysis. By combining electrochemical measurements with infrared spectroscopy of CO on Pt—an interface-specific probe sensitive to polarization—we establish that distributed Pt−liquid interfaces are spontaneously electrically polarized via equilibrated proton transfer in water and equilibrated electron transfer from organometallic redox buffers in an aprotic, organic *o*-DFB solvent. Despite the disparate mechanisms of polarization and the disparate reaction media, we find that both modes of polarization influence the catalytic rate of an explicitly nonpolar probe reaction—liquid-phase ethylene hydrogenation on Pt/C—with similar scale factors. This points toward a general electrostatic phenomenology that may be inherent to all catalysis at metal−liquid interfaces across diverse reaction media.

The foregoing understanding has important implications for mechanistic inquiry and the design of efficient catalytic processes. In particular, our findings highlight that the electrochemical potential of the catalyst, E_{OCP}—a generally overlooked parameter in heterogeneous catalysis—warrants consideration in mechanistic studies of reactions at solid−liquid interfaces. Moreover, our work establishes simple methods for leveraging electrostatics to complement existing chemical approaches to elucidating surface chemistry and designing catalytic interfaces. More broadly, given that spontaneous polarization is operative at distributed interfaces, our approach offers a straightforward and scalable strategy to impose oriented electric fields to manipulate preparative chemical transformations, a long-standing challenge in chemistry.[18,19] Indeed, this work highlights the value of merging concepts from the historically disparate communities of heterogeneous catalysis and electrochemistry in order to advance the science of catalysis in condensed-phase media.

ASSOCIATED CONTENT

Supporting Information

The Supporting Information is available free of charge at https://pubs.acs.org/doi/10.1021/acscentsci.1c00293.

Full experimental details, additional ATR-IR data, CO stripping data, additional rate data, additional E_{OCP} data, Pt particle size distributions, cyclic voltammograms (PDF)

AUTHOR INFORMATION

Corresponding Authors

Yuriy Román-Leshkov − *Department of Chemical Engineering, Massachusetts Institute of Technology, Cambridge, Massachusetts 02139, United States;* orcid.org/0000-0002-0025-4233; Email: yroman@mit.edu

Yogesh Surendranath − *Department of Chemistry, Massachusetts Institute of Technology, Cambridge, Massachusetts 02139, United States;* orcid.org/0000-0003-1016-3420; Email: yogi@mit.edu

Author

Thejas S. Wesley − *Department of Chemical Engineering, Massachusetts Institute of Technology, Cambridge, Massachusetts 02139, United States;* orcid.org/0000-0003-1989-6460

Complete contact information is available at: https://pubs.acs.org/10.1021/acscentsci.1c00293

Notes

The authors declare no competing financial interest.

ACKNOWLEDGMENTS

We gratefully acknowledge Sujay Bagi for performing TEM measurements. We also thank Patrick W. Smith, John R. Di Iorio, Michael L. Pegis, Jaeyune Ryu, Mark M. Sullivan, and Daniel T. Bregante for helpful technical advice and scientific discussions. We further thank J.R.D. and J.R. for valuable feedback on the manuscript. The electrochemical studies were supported by the Air Force Office of Scientific Research (AFOSR) under award number FA9550-20-1-0291. The thermochemical studies were supported by a Prof. Amar G. Bose Research Program Grant from MIT. T.S.W. acknowledges support from the National Science Foundation Graduate Research Fellowship under Grant No. 174530.

REFERENCES

(1) Stoukides, M.; Vayenas, C. G. The Effect of Electrochemical Oxygen Pumping on the Rate and Selectivity of Ethylene Oxidation on Polycrystalline Silver. *J. Catal.* **1981**, *70* (1), 137−146.

(2) Vayenas, C. G.; Bebelis, S.; Ladas, S. Dependence of Catalytic Rates on Catalyst Work Function. *Nature* **1990**, *343*, 625−627.

(3) Neophytides, S. G.; Tsiplakides, D.; Stonehart, P.; Jaksic, M. M.; Vayenas, C. G. Electrochemical Enhancement of a Catalytic Reaction in Aqueous Solution. *Nature* **1994**, *370*, 45−47.

(4) Vayenas, C. G.; Bebelis, S.; Pliangos, C.; Brosda, S.; Tsiplakides, D. *Electrochemical Activation of Catalysis: Promotion, Electrochemical Promotion, and Metal-Support Interactions*; Kluwer Academic/Plenum Publishers: New York, 2001.

(5) Wasileski, S. A.; Janik, M. J. A First-Principles Study of Molecular Oxygen Dissociation at an Electrode Surface: A Comparison of Potential Variation and Coadsorption Effects. *Phys. Chem. Chem. Phys.* **2008**, *10* (25), 3613−3627.

(6) Gorin, C. F.; Beh, E. S.; Kanan, M. W. An Electric Field-Induced Change in the Selectivity of a Metal Oxide-Catalyzed Epoxide Rearrangement. *J. Am. Chem. Soc.* **2012**, *134* (1), 186−189.

(7) Gorin, C. F.; Beh, E. S.; Bui, Q. M.; Dick, G. R.; Kanan, M. W. Interfacial Electric Field Effects on a Carbene Reaction Catalyzed by Rh Porphyrins. *J. Am. Chem. Soc.* **2013**, *135* (30), 11257−11265.

(8) Lau, V. M.; Gorin, C. F.; Kanan, M. W. Electrostatic Control of Regioselectivity via Ion Pairing in a Au(I)-Catalyzed Rearrangement. *Chem. Sci.* **2014**, *5*, 4975−4979.

(9) Klinska, M.; Smith, L. M.; Gryn'ova, G.; Banwell, M. G.; Coote, M. L. Experimental Demonstration of pH-Dependent Electrostatic Catalysis of Radical Reactions. *Chem. Sci.* **2015**, *6* (10), 5623−5627.

(10) Aragonès, A. C.; Haworth, N. L.; Darwish, N.; Ciampi, S.; Bloomfield, N. J.; Wallace, G. G.; Diez-Perez, I.; Coote, M. L. Electrostatic Catalysis of a Diels-Alder Reaction. *Nature* **2016**, *531* (7592), 88−91.

(11) Azcarate, I.; Costentin, C.; Robert, M.; Savéant, J.-M. Through-Space Charge Interaction Substituent Effects in Molecular Catalysis Leading to the Design of the Most Efficient Catalyst of CO_2-to-CO Electrochemical Conversion. *J. Am. Chem. Soc.* **2016**, *138* (51), 16639−16644.

(12) Beh, E. S.; Basun, S. A.; Feng, X.; Idehenre, I. U.; Evans, D. R.; Kanan, M. W. Molecular Catalysis at Polarized Interfaces Created by Ferroelectric $BaTiO_3$. *Chem. Sci.* **2017**, *8* (4), 2790−2794.

(13) Reath, A. H.; Ziller, J. W.; Tsay, C.; Ryan, A. J.; Yang, J. Y. Redox Potential and Electronic Structure Effects of Proximal Nonredox Active Cations in Cobalt Schiff Base Complexes. *Inorg. Chem.* **2017**, *56* (6), 3713−3718.
(14) Chantarojsiri, T.; Ziller, J. W.; Yang, J. Y. Incorporation of Redox-Inactive Cations Promotes Iron Catalyzed Aerobic C-H Oxidation at Mild Potentials. *Chem. Sci.* **2018**, *9* (9), 2567−2574.
(15) Kang, K.; Fuller, J.; Reath, A. H.; Ziller, J. W.; Alexandrova, A. N.; Yang, J. Y. Installation of Internal Electric Fields by Non-Redox Active Cations in Transition Metal Complexes. *Chem. Sci.* **2019**, *10* (43), 10135−10142.
(16) Goldsmith, Z. K.; Secor, M.; Hammes-Schiffer, S. Inhomogeneity of Interfacial Electric Fields at Vibrational Probes on Electrode Surfaces. *ACS Cent. Sci.* **2020**, *6* (2), 304−311.
(17) Warburton, R. E.; Hutchison, P.; Jackson, M. N.; Pegis, M. L.; Surendranath, Y.; Hammes-Schiffer, S. Interfacial Field-Driven Proton-Coupled Electron Transfer at Graphite-Conjugated Organic Acids. *J. Am. Chem. Soc.* **2020**, *142* (49), 20855−20864.
(18) Shaik, S.; Mandal, D.; Ramanan, R. Oriented Electric Fields as Future Smart Reagents in Chemistry. *Nat. Chem.* **2016**, *8* (12), 1091−1098.
(19) Shaik, S.; Danovich, D.; Joy, J.; Wang, Z.; Stuyver, T. Electric-Field Mediated Chemistry: Uncovering and Exploiting the Potential of (Oriented) Electric Fields to Exert Chemical Catalysis and Reaction Control. *J. Am. Chem. Soc.* **2020**, *142* (29), 12551−12562.
(20) Che, F.; Gray, J. T.; Ha, S.; Kruse, N.; Scott, S. L.; McEwen, J.-S. Elucidating the Roles of Electric Fields in Catalysis: A Perspective. *ACS Catal.* **2018**, *8* (6), 5153−5174.
(21) Fried, S. D.; Bagchi, S.; Boxer, S. G. Extreme Electric Fields Power Catalysis in the Active Site of Ketosteroid Isomerase. *Science* **2014**, *346* (6216), 1510−1514.
(22) Liu, C. T.; Layfield, J. P.; Stewart, R. J.; French, J. B.; Hanoian, P.; Asbury, J. B.; Hammes-Schiffer, S.; Benkovic, S. J. Probing the Electrostatics of Active Site Microenvironments along the Catalytic Cycle for Escherichia Coli Dihydrofolate Reductase. *J. Am. Chem. Soc.* **2014**, *136* (29), 10349−10360.
(23) Serrano-Ruiz, J. C.; Dumesic, J. A. Catalytic Routes for the Conversion of Biomass into Liquid Hydrocarbon Transportation Fuels. *Energy Environ. Sci.* **2011**, *4* (1), 83−99.
(24) Schutyser, W.; Renders, T.; Van den Bosch, S.; Koelewijn, S.-F.; Beckham, G. T.; Sels, B. F. Chemicals from Lignin: An Interplay of Lignocellulose Fractionation, Depolymerisation, and Upgrading. *Chem. Soc. Rev.* **2018**, *47*, 852−908.
(25) Sievers, C.; Noda, Y.; Qi, L.; Albuquerque, E. M.; Rioux, R. M.; Scott, S. L. Phenomena Affecting Catalytic Reactions at Solid-Liquid Interfaces. *ACS Catal.* **2016**, *6* (12), 8286−8307.
(26) Mondelli, C.; Gözaydin, G.; Yan, N.; Pérez-Ramírez, J. Biomass Valorisation over Metal-Based Solid Catalysts from Nanoparticles to Single Atoms. *Chem. Soc. Rev.* **2020**, *49* (12), 3764−3782.
(27) Keane, M. A. Catalytic Conversion of Waste Plastics: Focus on Waste PVC. *J. Chem. Technol. Biotechnol.* **2007**, *82*, 787−795.
(28) Celik, G.; Kennedy, R. M.; Hackler, R. A.; Ferrandon, M.; Tennakoon, A.; Patnaik, S.; Lapointe, A. M.; Ammal, S. C.; Heyden, A.; Perras, F. A.; Pruski, M.; Scott, S. L.; Poeppelmeier, K. R.; Sadow, A. D.; Delferro, M. Upcycling Single-Use Polyethylene into High-Quality Liquid Products. *ACS Cent. Sci.* **2019**, *5* (11), 1795−1803.
(29) Zhang, F.; Zeng, M.; Yappert, R. D.; Sun, J.; Lee, Y.-H.; LaPointe, A. M.; Peters, B.; Abu-Omar, M. M.; Scott, S. L. Polyethylene Upcycling to Long-Chain Alkylaromatics by Tandem Hydrogenolysis/Aromatization. *Science* **2020**, *370* (6515), 437−441.
(30) Rorrer, J. E.; Beckham, G. T.; Román-Leshkov, Y. Conversion of Polyolefin Waste to Liquid Alkanes with Ru-Based Catalysts under Mild Conditions. *JACS Au* **2021**, *1* (1), 8−12.
(31) Bockris, J. O.; Reddy, A.; Gamboa-Aldeco, M. *Modern Electrochemistry 2A: Fundamentals of Electrodics*, 2nd ed.; Springer: Boston, MA, 2000.
(32) Deshlahra, P.; Schneider, W. F.; Bernstein, G. H.; Wolf, E. E. Direct Control of Electron Transfer to the Surface-CO Bond on a Pt/TiO_2 Catalytic Diode. *J. Am. Chem. Soc.* **2011**, *133* (41), 16459−16467.
(33) Choksi, T.; Majumdar, P.; Greeley, J. P. Electrostatic Origins of Linear Scaling Relationships at Bifunctional Metal/Oxide Interfaces: A Case Study of Au Nanoparticles on Doped MgO Substrates. *Angew. Chem., Int. Ed.* **2018**, *57* (47), 15410−15414.
(34) Toney, M. F.; Howard, J. N.; Richer, J.; Borges, G. L.; Gordon, J. G.; Melroy, O. R.; Wiesler, D. G.; Yee, D.; Sorensen, L. B. Voltage-Dependent Ordering of Water Molecules at an Electrode-Electrolyte Interface. *Nature* **1994**, *368* (6470), 444−446.
(35) Ataka, K.; Yotsuyanagi, T.; Osawa, M. Potential-Dependent Reorientation of Water Molecules at an Electrode/Electrolyte Interface Studied by Surface-Enhanced Infrared Absorption Spectroscopy. *J. Phys. Chem.* **1996**, *100* (25), 10664−10672.
(36) Ledezma-Yanez, I.; Wallace, W. D. Z.; Sebastián-Pascual, P.; Climent, V.; Feliu, J. M.; Koper, M. T. M. Interfacial Water Reorganization as a pH-Dependent Descriptor of the Hydrogen Evolution Rate on Platinum Electrodes. *Nat. Energy* **2017**, *2*, 1−7.
(37) Limmer, D. T.; Willard, A. P.; Madden, P.; Chandler, D. Hydration of Metal Surfaces Can Be Dynamically Heterogeneous and Hydrophobic. *Proc. Natl. Acad. Sci. U. S. A.* **2013**, *110* (11), 4200−4205.
(38) Fumagalli, L.; Esfandiar, A.; Fabregas, R.; Hu, S.; Ares, P.; Janardanan, A.; Yang, Q.; Radha, B.; Taniguchi, T.; Watanabe, K.; Gomila, G.; Novoselov, K. S.; Geim, A. K. Anomalously Low Dielectric Constant of Confined Water. *Science* **2018**, *360* (6395), 1339−1342.
(39) Tian, Z.-Q.; Ren, B.; Chen, Y.-X.; Zou, S.-Z.; Mao, B.-W. Probing Electrode/Electrolyte Interfacial Structure in the Potential Region of Hydrogen Evolution by Raman Spectroscopy. *J. Chem. Soc., Faraday Trans.* **1996**, *92* (20), 3829−3838.
(40) Figueiredo, M. C.; Hiltrop, D.; Sundararaman, R.; Schwarz, K. A.; Koper, M. T. M. Absence of Diffuse Double Layer Effect on the Vibrational Properties and Oxidation of Chemisorbed Carbon Monoxide on a Pt(111) Electrode. *Electrochim. Acta* **2018**, *281*, 127−132.
(41) Resasco, J.; Chen, L. D.; Clark, E.; Tsai, C.; Hahn, C.; Jaramillo, T. F.; Chan, K.; Bell, A. T. Promoter Effects of Alkali Metal Cations on the Electrochemical Reduction of Carbon Dioxide. *J. Am. Chem. Soc.* **2017**, *139*, 11277−11287.
(42) Sarkar, S.; Patrow, J. G.; Voegtle, M. J.; Pennathur, A. K.; Dawlaty, J. M. Electrodes as Polarizing Functional Groups: Correlation between Hammett Parameters and Electrochemical Polarization. *J. Phys. Chem. C* **2019**, *123* (8), 4926−4937.
(43) Schmickler, W.; Santos, E. *Interfacial Electrochemistry*, 2nd ed.; Springer: Heidelberg, 2010.
(44) Callen, H. B. *Thermodynamics and an Introduction to Thermostatistics*, 2nd ed.; Wiley, 1985.
(45) Ryu, J.; Surendranath, Y. Tracking Electrical Fields at the Pt/H_2O Interface during Hydrogen Catalysis. *J. Am. Chem. Soc.* **2019**, *141* (39), 15524−15531.
(46) Lamy-Pitara, E.; El Mouahid, S.; Barbier, J. Effect of Anions on Catalytic and Electrocatalytic Hydrogenations and on the Electrocatalytic Oxidation and Evolution of Hydrogen on Platinum. *Electrochim. Acta* **2000**, *45* (25−26), 4299−4308.
(47) Ebbesen, S. D.; Mojet, B. L.; Lefferts, L. In Situ ATR-IR Study of CO Adsorption and Oxidation over Pt/Al_2O_3 in Gas and Aqueous Phase: Promotion Effects by Water and pH. *J. Catal.* **2007**, *246* (1), 66−73.
(48) Ebbesen, S. D.; Mojet, B. L.; Lefferts, L. The Influence of Water and pH on Adsorption and Oxidation of CO on Pd/Al_2O_3-an Investigation by Attenuated Total Reflection Infrared Spectroscopy. *Phys. Chem. Chem. Phys.* **2009**, *11* (4), 641−649.
(49) Singh, N.; Lee, M.-S.; Akhade, S. A.; Cheng, G.; Camaioni, D. M.; Gutiérrez, O. Y.; Glezakou, V.-A.; Rousseau, R.; Lercher, J. A.; Campbell, C. T. Impact of pH on Aqueous-Phase Phenol Hydrogenation Catalyzed by Carbon-Supported Pt and Rh. *ACS Catal.* **2019**, *9*, 1120−1128.

https://doi.org/10.1021/acscentsci.1c00293
ACS Cent. Sci. XXXX, XXX, XXX−XXX

(50) Gileadi, E. *Physical Electrochemistry: Fundamentals, Techniques and Applications*; Wiley-VCH: Weinheim, 2011.
(51) Beden, B.; Bewick, A.; Lamy, C. A Study by Electrochemically Modulated Infrared Reflectance Spectroscopy of the Electrosorption of Formic Acid at a Platinum Electrode. *J. Electroanal. Chem. Interfacial Electrochem.* **1983**, *148* (1), 147−160.
(52) Chang, S.-C.; Weaver, M. J. Coverage-Dependent Dipole Coupling for Carbon Monoxide Adsorbed at Ordered Platinum(111)-Aqueous Interfaces: Structural and Electrochemical Implications. *J. Chem. Phys.* **1990**, *92* (7), 4582−4594.
(53) Rice, C.; Tong, Y.; Oldfield, E.; Wieckowski, A.; Hahn, F.; Gloaguen, F.; Léger, J.-M.; Lamy, C. In Situ Infrared Study of Carbon Monoxide Adsorbed onto Commercial Fuel-Cell-Grade Carbon-Supported Platinum Nanoparticles: Correlation with ^{13}C NMR Results. *J. Phys. Chem. B* **2000**, *104* (24), 5803−5807.
(54) Arenz, M.; Mayrhofer, K. J. J.; Stamenkovic, V.; Blizanac, B. B.; Tomoyuki, T.; Ross, P. N.; Markovic, N. M. The Effect of the Particle Size on the Kinetics of CO Electrooxidation on High Surface Area Pt Catalysts. *J. Am. Chem. Soc.* **2005**, *127* (18), 6819−6829.
(55) Vuissoz, P.-A.; Ansermet, J.-P.; Wieckowski, A. Probing by NMR the Effect of Surface Charges on the Chemisorption Bond. *Phys. Rev. Lett.* **1999**, *83* (12), 2457−2460.
(56) Marković, N. M.; Lucas, C. A.; Rodes, A.; Stamenković, V.; Ross, P. N. Surface Electrochemistry of CO on Pt(111): Anion Effects. *Surf. Sci.* **2002**, *499* (2−3), L149−L158.
(57) McPherson, I. J.; Ash, P. A.; Jacobs, R. M. J.; Vincent, K. A. Formate Adsorption on Pt Nanoparticles during Formic Acid Electro-Oxidation: Insights from in Situ Infrared Spectroscopy. *Chem. Commun.* **2016**, *52* (85), 12665−12668.
(58) Ebbesen, S. D.; Mojet, B. L.; Lefferts, L. CO Adsorption and Oxidation at the Catalyst-Water Interface: An Investigation by Attenuated Total Reflection Infrared Spectroscopy. *Langmuir* **2006**, *22* (3), 1079−1085.
(59) Park, S.; Tong, Y.; Wieckowski, A.; Weaver, M. J. Infrared Reflection-Absorption Properties of Platinum Nanoparticle Films on Metal Electrode Substrates: Control of Anomalous Optical Effects. *Electrochem. Commun.* **2001**, *3* (9), 509−513.
(60) Pecharromán, C; Cuesta, A; Gutiérrez, C. Comments on the paper by M.-S. Zheng and S.-G. Sun entitled "In Situ FTIR Spectroscopic Studies of CO Adsorption on Electrodes with Nanometer-Scale Thin Films of Ruthenium in Sulfuric Acid Solutions. *J. Electroanal. Chem.* **2002**, *529* (2), 145−154.
(61) Pecharromán, C.; Cuesta, A.; Gutiérrez, C. Calculation of Adsorption-Induced Differential External Reflectance Infrared Spectra of Particulate Metals Deposited on a Substrate. *J. Electroanal. Chem.* **2004**, *563* (1), 91−109.
(62) McPherson, I. J.; Ash, P. A.; Jones, L.; Varambhia, A.; Jacobs, R. M. J.; Vincent, K. A. Electrochemical CO Oxidation at Platinum on Carbon Studied through Analysis of Anomalous in Situ IR Spectra. *J. Phys. Chem. C* **2017**, *121* (32), 17176−17187.
(63) Van Der Niet, M. J. T. C.; Garcia-Araez, N.; Hernández, J.; Feliu, J. M.; Koper, M. T. M. Water Dissociation on Well-Defined Platinum Surfaces: The Electrochemical Perspective. *Catal. Today* **2013**, *202* (1), 105−113.
(64) Müller, E.; Schwabe, K. Katalytische Spaltung und Oxydation der Ameisensäure. *Zeitschrift für Elektrochemie und angewandte physikalische Chemie* **1928**, *34*, 170−185.
(65) Mallat, T.; Baiker, A. Catalyst Potential Measurement: A Valuable Tool for Understanding and Controlling Liquid Phase Redox Reactions. *Top. Catal.* **1999**, *8*, 115−124.
(66) Cortright, R. D.; Goddard, S. A.; Rekoske, J. E.; Dumesic, J. A. Kinetic Study of Ethylene Hydrogenation. *J. Catal.* **1991**, *127* (1), 342−353.
(67) Mears, D. E. Tests for Transport Limitations in Experimental Catalytic Reactors. *Ind. Eng. Chem. Process Des. Dev.* **1971**, *10* (4), 541−547.
(68) Madon, R. J.; Boudart, M. Experimental Criterion for the Absence of Artifacts in the Measurement of Rates of Heterogeneous Catalytic Reactions. *Ind. Eng. Chem. Fundam.* **1982**, *21* (4), 438−447.
(69) Koros, R. M.; Nowak, E. J. A Diagnostic Test of the Kinetic Regime in a Packed Bed Reactor. *Chem. Eng. Sci.* **1967**, *22* (3), 470.
(70) Jackson, M. N.; Jung, O.; Lamotte, H. C.; Surendranath, Y. Donor-Dependent Promotion of Interfacial Proton-Coupled Electron Transfer in Aqueous Electrocatalysis. *ACS Catal.* **2019**, *9* (4), 3737−3743.
(71) Gast, J. A.; Thompson, T. G. Evaporation of Boric Acid from Sea Water. *Tellus* **1959**, *11* (3), 344−347.
(72) Wieckowski, A.; Rosasco, S. D.; Salaita, G. N.; Hubbard, A.; Bent, B. E.; Zaera, F.; Somorjai, G. A. Comparison of Gas-Phase and Electrochemical Hydrogenation of Ethylene at Platinum Surfaces. *J. Am. Chem. Soc.* **1985**, *107* (21), 5910−5920.
(73) O'Toole, T. R.; Younathan, J. N.; Sullivan, B. P.; Meyer, T. J. 1,2-Difluorobenzene: A Relatively Inert and Noncoordinating Solvent for Electrochemical Studies on Transition-Metal Complexes. *Inorg. Chem.* **1989**, *28* (20), 3923−3926.
(74) Roth, J. D.; Weaver, M. J. Role of the Double-Layer Cation on the Potential-Dependent Stretching Frequencies and Binding Geometries of Carbon Monoxide at Platinum-Nonaqueous Interfaces. *Langmuir* **1992**, *8* (5), 1451−1458.
(75) Vayenas, C. G.; Bebelis, S.; Neophytides, S. Non-Faradaic Electrochemical Modification of Catalytic Activity. *J. Phys. Chem.* **1988**, *92* (18), 5083−5085.
(76) Bebelis, S.; Vayenas, C. G. Non-Faradaic Electrochemical Modification of Catalytic Activity. 1. The Case of Ethylene Oxidation on Pt. *J. Catal.* **1989**, *118* (1), 125−146.
(77) Fletcher, S. Tafel Slopes from First Principles. *J. Solid State Electrochem.* **2009**, *13*, 537−549.
(78) Zope, B. N.; Hibbitts, D. D.; Neurock, M.; Davis, R. J. Reactivity of the Gold/Water Interface During Selective Oxidation Catalysis. *Science* **2010**, *330* (6000), 74−78.
(79) Wieckowski, A.; Neurock, M. Contrast and Synergy between Electrocatalysis and Heterogeneous Catalysis. *Adv. Phys. Chem.* **2011**, *2011*, 1−18.
(80) Wilson, N. M.; Flaherty, D. W. Mechanism for the Direct Synthesis of H_2O_2 on Pd Clusters: Heterolytic Reaction Pathways at the Liquid-Solid Interface. *J. Am. Chem. Soc.* **2016**, *138* (2), 574−586.
(81) Adams, J. S.; Chemburkar, A.; Priyadarshini, P.; Ricciardulli, T.; Lu, Y.; Maliekkal, V.; Sampath, A.; Winikoff, S.; Karim, A. M.; Neurock, M.; Flaherty, D. W. Solvent Molecules Form Surface Redox Mediators in Situ and Cocatalyze O_2 Reduction on Pd. *Science* **2021**, *371* (6529), 626−632.
(82) Yang, G.; Akhade, S. A.; Chen, X.; Liu, Y.; Lee, M.-S.; Glezakou, V.-A.; Rousseau, R.; Lercher, J. A. The Nature of Hydrogen Adsorption on Platinum in the Aqueous Phase. *Angew. Chem., Int. Ed.* **2019**, *58* (11), 3527−3532.
(83) Madon, R. J.; Iglesia, E. Catalytic Reaction Rates in Thermodynamically Non-Ideal Systems. *J. Mol. Catal. A: Chem.* **2000**, *163* (1−2), 189−204.

https://doi.org/10.1021/acscentsci.1c00293
ACS Cent. Sci. XXXX, XXX, XXX−XXX